This updated document was made available on 27th September 2022.

Supporting Information

A Self-healing, Recyclable and Conductive Gelatin/Nanofibrillated Cellulose/Fe^{3+} Hydrogels Based on Multi-Dynamic Interactions for Multifunctional Strain Sensor

Haocheng Fu, Bin Wang*, Jinpeng Li*, Jun Xu*, Jun Li, Jinsong Zeng, Wenhua Gao and Kefu Chen

Plant Fiber Material Science Research Center, State Key Laboratory of Pulp and Paper Engineering, South China University of Technology, Guangzhou 510640, P.R. China;
Corresponding authors
*Bin Wang, E-mail: febwang@scut.edu.cn
*Jinpeng Li, E-mail: ljp@scut.edu.cn
*Jun Xu, E-mail: xujun@scut.edu.cn

Experimental Section

Materials. The cellulose fiber obtained from bleached softwood pulp was supplied by Hubei Chemical Fiber Co., Ltd., China. TEMPO (purity ≥98 %) was obtained from Sigma-Aldrich (St. Louis, MO, USA). Sodium hydroxide (NaOH, purity ≥97 %), sodium bromide (NaBr, purity ≥99 %) and $FeCl_3$ were purchased from Fu Chen (Tian Jin) Chemical Reagent Co., Ltd. Sodium hypochlorite (NaClO) solution (active chlorine content ≥7.50 %) was purchased from Guangdong Guangshi reagent Technology Co., Ltd. Ethanediol (purity ≥98%) was purchased from Sinopharm Chemical Reagent Co., Ltd. (Shanghai, China). The gelatin (~300 g Bloom) was purchased from Beijing Jinming Biotechnology Co., Ltd. The glue stick (7102) and glue (7302) were purchased from Deli Group Co., Ltd (Ningbo, China). The other all reagents were purchased from Macklin (Shanghai, China).

Preparation of Nanofibrillated Cellulose. The cellulose fiber was oxidized by the TEMPO/NaBr/NaClO system under the condition of alkaline. In brief, 160 g of cellulose fibers and 14.64 L of water were added to a 22 L bucket. Afterward, 2.56 g 2,2,6,6-tetramethylpyperidine-1-oxyl (TEMPO) (0.016 g/g cellulose fibers) and 16.00 g NaBr (0.10 g/g cellulose fibers) were added to the bucket. The TEMPO-mediated oxidation was triggered by adding unopened NaClO solution (1.00 mmol/g cellulose fibers) to the suspension. The pH value of the oxidation system was maintained at 10.0 by adding NaOH solution (0.50 mol/L). The mixture was stirred at 500 r/min for 1 h and was terminated by adding 40.00 mL of alcohol. The suspension was filtered and washed with deionized water until pH became neutral. The filtrate was diluted to 1 wt% with deionized water and then defibrillated through a Supermasscolloider grinder (MKCA6-2J Masuko Sangyo Co., LTD, Japan) at 2400 rpm with a millstone gap of -100 μm. The final slurry was collected and defined as TEMPO-oxidized nanofibrillated cellulose (TNFC).

Synthesis of Dialdehyde TNFC. In order to make full use of the free hydroxyl groups at C_2 and C_3 of TNFC, 15 g $NaIO_4$ was added to 1000 g TNFC suspension (1.0 wt%), and the mixture was stirred by vigorous mechanical agitation in the absence of light for 3 h at 60 °C. The reaction was quenched by adding 20 mL glycol followed by centrifugating six times to remove remaining reagents. The precipitate was collected and named as Dialdehyde TNFC (DATNFC, 78.0 % yield from TNFC).

Preparation of nanocomposite hydrogels. The nanocomposite hydrogels were prepared by sol-gel method followed by ion-dipping approach. Initially, 10 g gelatin (absolutely dry) was dissolved in distilled water at 400 rpm under 45 °C. Then 2~15 wt% of DATNFC suspension (based on gelatin) was slowly added into the gelatin solution. The mixture was magnetically stirred for 1 h at 45 °C to obtain a homogeneous dispersion, while the concentration of gelatin in water was kept at 10 wt%. The mixture was poured into different molds at 4 °C to form dumbbell shaped and cylindrical

gelatin/DATNFC hydrogel (GDH). The dumbbell shaped and cylindrical GDH with 10 % content of DATNFC was immersed in different concentrations of $FeCl_3$ solution (0.02, 0.04, 0.06, 0.08 and 0.10 mol/L) for 24 h and 48 h, respectively to make sure the complete crosslinking between Fe^{3+} and -COOH (0.33 mmol/g, Table S1).[1] The final composite hydrogel was stored in sealed foam box at 4 °C.

Determination of Carboxyl and Aldehyde Contents. The carboxyl content of TNFC was calculated by conductometric titration. In short, 0.25 g freeze-dried samples were immersed into HCl solution (15 mL, 0.01 mol/L) for 1 h. The soaked sample was washed by deionized water, and then resuspended in 0.001 mol/L NaCl solution. Here, 200 μL HCl solution (0.1 mol/L) was added to mixture before titration. Conductivity was measured after adding NaOH solution (50 μL, 0.1 mol/L) when the meter (ZetaProbe 7020 with conductivity probe) exhibited a stable number. The carboxyl content was determined by equation (1):

$$\text{Carboxyl content} = (C_{NaOH} \times V_{NaOH})/Ws \text{ (mmol/g)} \quad (1)$$

where C_{NaOH} means the concentration of titrant (mol/L), V_{NaOH} is the consumed volume of NaOH at the equivalence point (mL), and Ws is dried weight of TNFC utilized for titration.

Aldehyde content (AC) was performed utilizing hydroxylamine hydrochloride titration method. The reaction principle is that dialdehyde group reacts with hydroxylamine hydrochloride to form oxime and generate HCl and H_2O. Firstly, 0.4 g of DATNFC was added to hydroxylamine hydrochloride (15 ml, 0.25 mol/L, pH=3.15) for 36 h at room temperature. Then, the mixture was titrated by 0.1 mol / L NaOH until the pH value reaches 3.15. The reaction principle and calculation formula are as follows:

$-CHO + NH_2OH \cdot HCl \rightarrow -CHNOH + HCl + H_2O$

$HCl + NaOH \rightarrow NaCl + H_2O$

$$AC = CV/m \text{ (mmol/g)} \quad (2)$$

where AC means the content of the aldehyde groups of DANFC (mmol/g); C and V are the normality of NaOH (0.05 mol/L) and the consumed volume of NaOH solution,

respectively.

Crosslinking index of GDH. The crosslinking index between gelatin and DATNFC was determined by the Ninhydrin colorimetry[1]. Ninhydrin reagent was prepared as follows: Solution A was prepared by mixing 25 mL deionized water containing 1.05 g citric acid, 0.03 g $SnCl_2$ and 0.40 g NaOH, while solution B contains 25 mL ethylene glycol methyl ether with 1 g Ninhydrin colorimetry. Two solutions were uniformly mixed in a dark bottle under magnetic stirring for 45 min. 10 mL mixed liquid with 15 mg dried sample was heated in a water bath at 80 °C for 30 min. The solution was cooled down to room temperature, followed by diluting with 50% (v/v) isopropanol. The content of amino group was determined by the absorbance at the wavelength of 570 nm by a spectrophotometer (UV-2600, Japan) due to the fact that the amino groups in hydrogels were directly proportional to the absorbance of solution. The experiments were repeated five times to determine the reliability of the data. The crosslinking degree was calculated according to the following equation:[2, 3]

$$\text{Crosslinking index (\%)} = (A_{non\text{-}c}\text{-}A_c)/A_{non\text{-}c} \times 100 \quad (3)$$

where $A_{non\text{-}c}$ means the absorbance of crosslinked hydrogel, A_c is the absorbance of non-crosslinked hydrogel.

General Characterization. The Fourier transform infrared (FT-IR) spectra of TNFC, DATNFC, Gelatin and nanocomposite hydrogel were conducted by FT-IR spectrometer (VERTEX 33, Bruker, USA). The morphology of DATNFC was determined by atomic force microscopy (AFM, Bruker, Germany). The crystalline structures of TNFC and DATNFC were ascertained using X-ray diffractometer (XRD) on a D8 ADVANGE diffractometer (Bruker, Germany) with a Cu Ka radiation (λ = 0.154 nm), operating at 40 kV with a filament of 40 mA.[4] The functional group of nanocomposite hydrogels was recognized by X-ray photoelectron spectroscopy (XPS) with monochromatic Al Kα (1486.6 eV) radiation as the excitation source. The thermal stability of nanocomposite hydrogel was evaluated using a TA Q500 analyzer (TA Instruments, New Castle, DE, USA). The transmittance of nanocomposite hydrogels

(40 × 10 × 2 mm^3) was determined by a spectrophotometer (UV-2600, Japan). The internal structure of nanocomposite hydrogel was broken after rapid frozen by liquid nitrogen, and then the freeze-dried samples were coated with gold for field-emission scanning electron microscopy (FE-SEM Merlin, Zeiss, Germany).

Mechanical Testing. The tensile and cyclic tensile (10 loading-unloading cycles after 3 pre-cycles at the strain of 30 %) tests were performed on the dumbbell shaped specimens (2 mm in height) using a tensile machine (INSTRON 5565) with a 500 N load cell at a rate of 10 mm/min, and the clamp span of device was 25 mm. The compressive and cycles compressive (10 loading-unloading cycles after 3 pre-cycles under the strain of 40 %) tests were performed on the cylindrical specimens (25 mm in diameter and 20 mm in height) using the machine (INSTRON 5565) with a 5 kN load cell at a rate of 10 mm/min.

Conductivity of nanocomposite hydrogel. The conductivity of the cylindrical composite hydrogels was measured by electrochemical impedance spectroscopy (EIS) measurement under the condition of 25 °C and 35 % relative humidity. The achievement of measuring instrument depended on electrochemical workstation (CHI660E, Shanghai) underwent the current ranging of 200 mA, and the frequency range from 1 Hz to 1 MHz. The sample was cut into pieces of 11 mm × 6 mm × 6 mm and sandwiched by copper tapes. The voltage of the current test for pressure sensor is 1 V. The conductivity was calculated by equation (4):

$$\rho^{-1}=L/(s\times R)=L/(s\times Z') \quad (4)$$

where ρ means the resistivity of hydrogel, L is the effective length of sample pieces, s, R and Z' represent the cross-sectional area, resistance, real part of impedance of sample, respectively.

Strain Sensitivity. The real time current of composite hydrogel under different strains was recorded by electrochemical workstation at 2 V voltage. The compressive sensitivity (S) was defined by the slope of the resistance change curve under

compressive test. The strain sensitivity in the process of tensile testing was calculated by equation (5):

$$GF=((R-R_0)/R_0)/\varepsilon \quad (5)$$

where R_0 and R are the initial resistance and that under strain, and ε is the strain of the hydrogel.

***Demonstration for Practical Application*.** Here, a simple encapsulation method was performed to reduce the evaporation of water, which can enhance the structural stability of hydrogel sensors. Moreover, the practical applications of hydrogel sensor were carried out at 20 ± 5 °C (Fig. S1a). After 168 h, the water loss of encapsulated GDIH10-0.06 was only 0.54 % (Fig. S1b). The sensor (25 × 10 × 2 mm^3) from dumbbell shaped GDIH10-0.06, acted as an ionic conductor, was used to prepare wearable strain sensor. As shown in Fig. S2a, the nanocomposite hydrogel was placed on two copper sheets, and was enwrapped by 3M VHB tapes. The as-prepared strain sensor was adhered on the volunteer's forefinger, knee, elbow joint and throat to monitor the various human motions. The real-time electrical signal changes caused by different motions were obtained from electrochemical workstation at 2V voltage. Similarly, the GDIH10-0.06 (20 × 20 × 2 mm^3) was used to discern handwritings and recognize personal signatures by applying the PFT types as the capsulation layers where the hydrogel sensor was enwrapped by scotch tapes (Fig. S2b). Finally, a hydrogel array (4 × 4) from cylindrical GDIH10-0.06 was designed to detect 2D distribution of force and strain, which was widely pursued for electronic skin where the size of GDIH10-0.06 was (5 × 5 × 4 mm^3). Similarly, the hydrogel array was encapsulated by scotch tapes.

Self-healing Process of fractured Strain Sensors. The dumbbell shaped composite hydrogel was cut into two parts, and then two cutting surfaces were closely contacted together at 40 °C for 60 s followed by a standing process at room temperature for 10 min. The obtained self-healed samples were stored in sealed foam box over night at 4 °C.[5, 6]

The recyclability of Strain sensors. The abandoned cylindrical and dumbbell shaped GDIH10-0.06 were dispersed in water at 45 °C for 60 min under 800 rpm to obtain uniform gel solution and adhesive, respectively. The concentration of recycled gelatin in water was kept at 6.0 wt%. The gel solution was poured into a mold at 4 °C to form recycled G_6DIH10-0.06. The mechanical properties and electrochemical behavior of the recycled hydrogel were tested according to the original hydrogel. The reconstituted adhesive (5.5 wt%), sticky tape, and glue was utilized to adhere the paper, glass, copper, iron and plastic. Moreover, the recycled hydrogel was coated on the substrate where the coating area is 2.0 × 1.8 m2 (copper) and 2.0 × 1.5 m2 (paper), respectively, and then another same substrate was placed on the coating area. The shear strength of reconstituted adhesive was assessed by mechanical test (INSTRON 5565) after the natural cooling of the adhesive

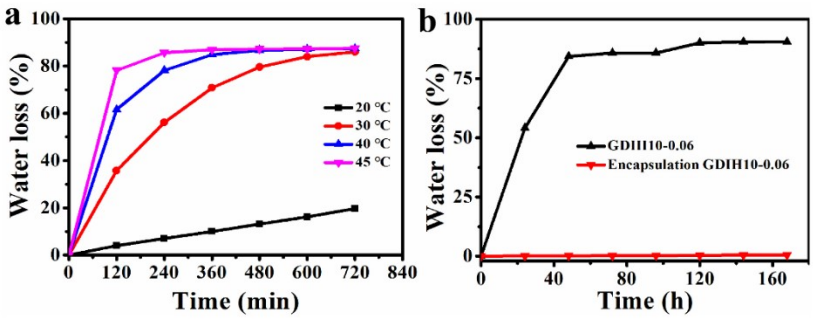

Fig. S1 (a) The water loss (%) of unencapsulated GDIH10-0.06 at different temperature after 720 min. (b) The water loss (%) of encapsulated GDIH10-0.06 at 20 °C after 168 h.

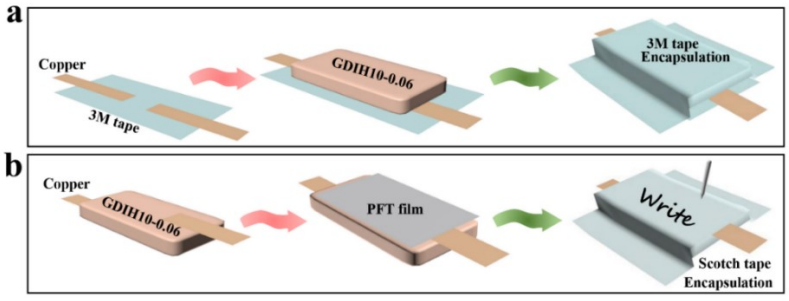

Fig. S2 Illustration of the assembly of (a) wearable strain sensors and (b) writing anti-counterfeiting devices by encapsulation.

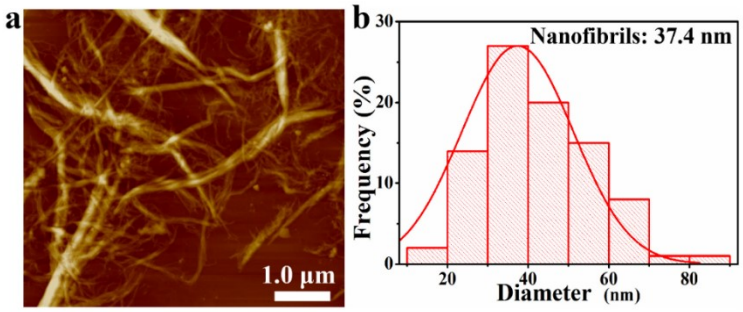

Fig. S3 AFM image (a) and average diameter (b) of DATNFC.

The FTIR spectrum was employed to determine the successful crosslinking of gelatin and DATNFC. As shown in Fig. S4, the absorbance peaks of TNFC and DATNFC at 3454, 2902, 1620, 1421, 1030, 897 cm^{-1} were corresponding to the -O-H stretching vibrations, symmetric -C-H vibrations, the symmetric stretching vibration of the carbonyl group, -OH stretching bands, -C-O-C- pyranose ring skeletal vibration and β-glycosidic linkages, respectively.[7, 8] The absorbance peak at 1732 cm^{-1} (the -C=O stretching vibration) of DATNFC indicated that the formation of aldehyde carbonyl groups in the process of dialdehyde oxidization. From the FTIR spectrum of pure gelatin, the absorbance peaks at 1653 cm^{-1}, 1543 cm^{-1}, and 1238 cm^{-1} were attributed to the C=O stretching vibration of amide I, N-H bending vibration of amide II, and in-plane bending of amide III, respectively. The absorbance peak of Schiff base could be found at 1650-1600 cm^{-1} (the C=N stretching vibration), while it was covered by the amide I of gelatin.[9, 10] In addition, the disappearance of absorbance peak at 1732 cm^{-1} showed that the aldehyde groups were consumed due to the reaction between DANFC and gelatin.

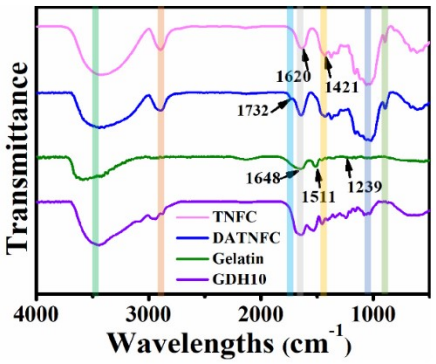

Fig. S4 FT-IR spectrum of the gelatin, TNFC, DATNFC and GDH10.

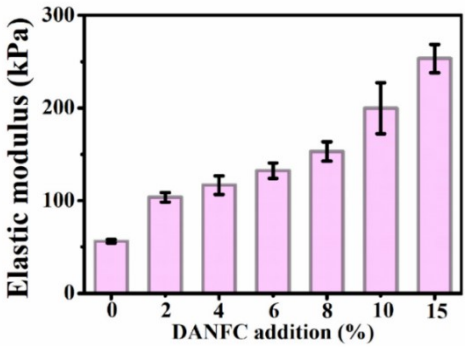

Fig. S5 The elastic modulus of nanocomposite hydrogel.

Considering the fluidity of mixture, GDH10 was finally selected to fabricate the composite hydrogel containing Fe^{3+}. The physical structure of nanocomposite hydrogel was analyzed by XRD pattern. The crystal structure of TNFC, DATNFC, gelatin, GDH10 and GDIH10-0.06 was presented in Fig. S6. The XRD pattern of TNFC and DATNFC displayed diffraction peaks at 2θ=15.05°, 16.40°, 22.62° and 34.27° corresponding to the typical cellulose I crystalline structure. The crystallinity index was calculated by the equation of "CrI (%) =$(1-I_{am}/I_{200})$ ×100", where I_{200} is the maximum intensity at 2θ = 22.6 °, which represents both crystalline and amorphous components, while I_{am} is the minimum intensity at 2θ = 18°, representing the amorphous fraction.[11] The crystallinity index (CrI) of TNFC and DATNFC was 69.7 and 66.9 % (Table S1), showing that the degree of crystallinity was slightly decreased after $NaIO_4$ oxidation.[7] After the addition of DATNFC and Fe^{3+}, there was a wide peak could be found from 20° to 25° in the XRD pattern of GDH10 and GDIH10-0.06. The result demonstrated that the introduction of DATNFC and Fe^{3+} exerted a poor effect on the crystalline form.

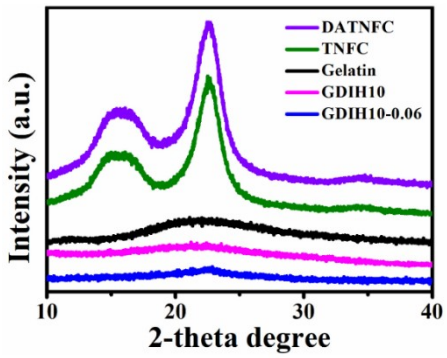

Fig. S6 The XRD pattern of TNFC, DATNFC, gelatin and nanocomposite hydrogel.

The distribution of N and Fe element in the composite hydrogel could be observed by EDS element mapping of GDIH10-0.06 (Fig. S7a). It demonstrated that the iron element (Fe) and nitrogen element (N) were distributed in the nanocomposite hydrogel uniformly, proving that gelatin and Fe^{3+} were symmetrically described in the composite hydrogel without obvious aggregation. Moreover, XPS was conducted to furtherly determine the chemical status of C, N, O, and Fe element in composite hydrogel. As shown in Fig. S7b, GDH10 and GDIH10 showed a predominant C 1s, O 1s and N 1s peak at around 283.0 eV, 529.1 eV and 397.9 eV, respectively, and an obvious Fe 2p peak (around 707.6 eV) could be found in the XPS spectra of nanocomposite hydrogel. The high-resolution C 1s, O 1s, Fe 2p and N 1s spectra of GDIH10-0.06 were presented in Fig. S7c-f, the C 1s spectrum of GDIH10-0.06 could be fitted to four peaks attributing to -O-C=O, -C-O, -C=N and -C-C at 288.5, 287.8, 286.2 and 284.7 eV, respectively.[12] Similarly, the O 1s spectrum could be distinguished as three peaks, centered at the binding energy of 532.0, 531.4 and 530.6 eV, attributing to -C-OH, -COOH and -C-O-C, respectively.[7] In addition, Fe 2p could be cure-fitted to two peaks at 724.4 and 711.0, while the N 1s could be fitted to two peaks attributing to -C-N/-C=N and -N-H, respectively[13-15]. Therefore, the hydroxyl, carboxyl and aldehyde groups in DATNFC could form dynamic interfacial interactions with hydroxyl, amino ($-NH_2$) in gelatin and Fe^{3+}, including Schiff base reaction, hydrogen bonds, and coordination bonds.

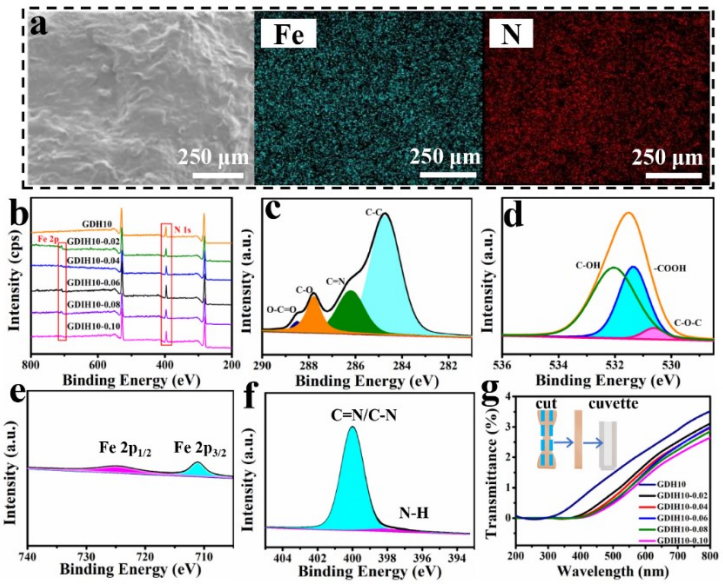

Fig. S7 (a) EDS images of GDIH10-0.06. (b) XPS spectra of nanocomposite hydrogel. High-resolution (c) C 1s, (d) O 1s, (e) Fe 2p and (f) N 1s of GDIH10-0.06. (g) The transmittance of nanocomposite hydrogel.

As illustrated in Fig. S6g, the transmittance of GDIH (40 × 10 × 2 mm^3) also showed a downward trend with the increasing content of Fe^{3+} from 0 to 0.10 mol/L in the visible spectral range. After dipping in Fe^{3+}, the coordination bond was formed within the GDIH matrix, and the color of the hydrogel turned from light-yellow to deep brown (Fig. S8a). However, in the UV spectral range, the transmittance sharply decreased to 0. It was apparent that nanocomposite hydrogel became darker with the increasing of Fe^{3+} under the irradiation of ultraviolet light at the wavelength of 254 and 365 nm, respectively (Fig. S8b). The main fact of transmittance reduction was the color of Fe^{3+}. On the other hand, the formation of more complex polymer networks could block the light passing through them.[16] Therefore, the developed GDIH possessed higher UV shielding of nanocomposite hydrogel, which protected living skin cells against UV radiation.

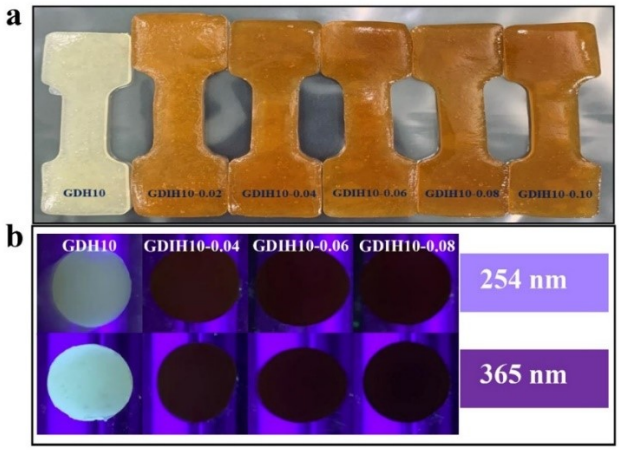

Fig. S8 (a) The optical photo of nanocomposite hydrogel. (b) The optical photos of nanocomposite hydrogel under UV irradiation at 254 nm and 365 nm, respectively.

The thermal stability was used to evaluate the effect of Fe^{3+} content on the structural properties of nanocomposite hydrogel. As shown in Fig. S9, weight loss of composite hydrogel had a downward trend with the increasing of Fe^{3+} content, and there was a decreasing trend first and then increasing in DTG curves. The temperature at 50 % mass loss ($T_{50\ \%}$), maximum degradation rate temperature (T_{max}) and the residual mass of

nanocomposite hydrogel were summarized in Table S2. The result showed that the trend of T_{max} was similar to that of DTG curves with the increasing of Fe^{3+}. It was obvious that the $T_{50\,\%}$ and residual mass of composite hydrogel were increased by Fe^{3+}, showing that the thermal stability of composite hydrogel was enhanced by Fe^{3+}. This was probably because that a stable network structure was formed by gelatin, Fe^{3+} and DANFC.[17]

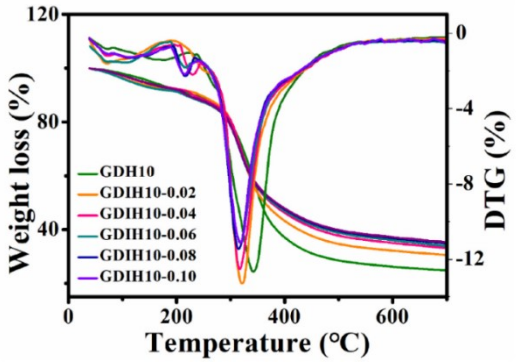

Fig. S9 The thermal stability of nanocomposite hydrogel.

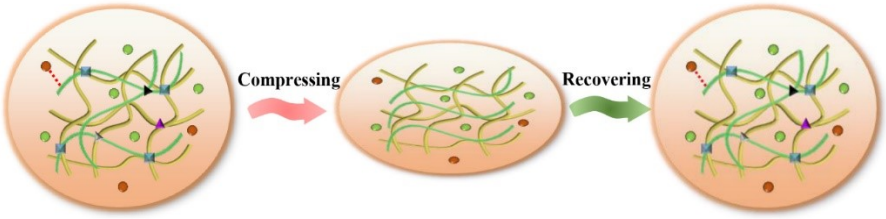

Fig. S10 Energy dissipation mechanism of the double network during compressive test.

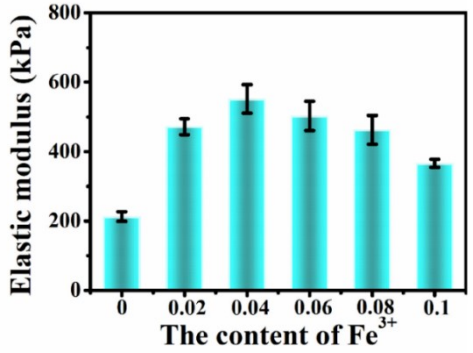

Fig. S11 The elastic modulus of nanocomposite hydrogel containing Fe^{3+}.

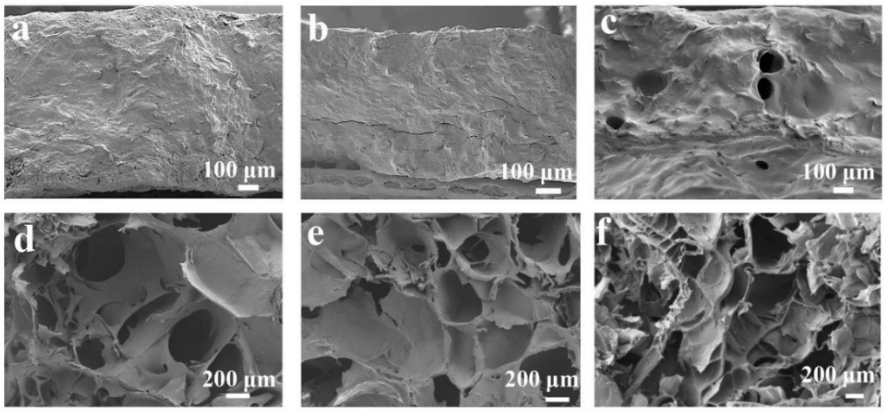

Fig. S12 The FE-SEM images of GDIH10-0.06 after tensile test: (a) original, (b) after one cyclic stretching-recovering, (c) after breaking. The FE-SEM images of GDIH10-0.06 after compression test: (d) original, (e) after one cyclic compressing-recovering, (f) after breaking.

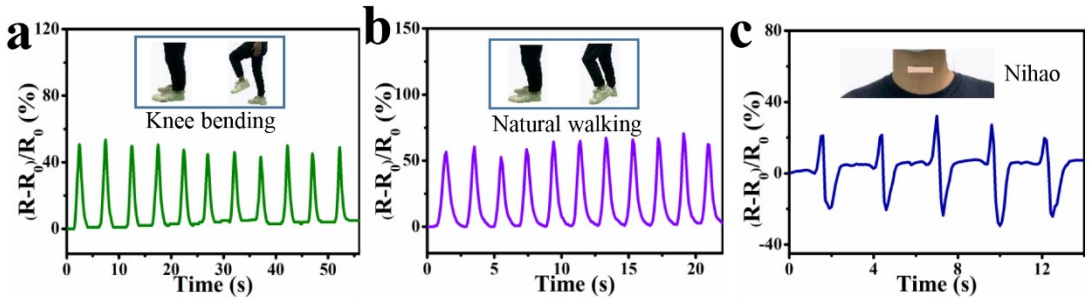

Fig. S13 The recorded relative resistance changes of GDIH10-0.06 for knee bending and throat vibrating, respectively.

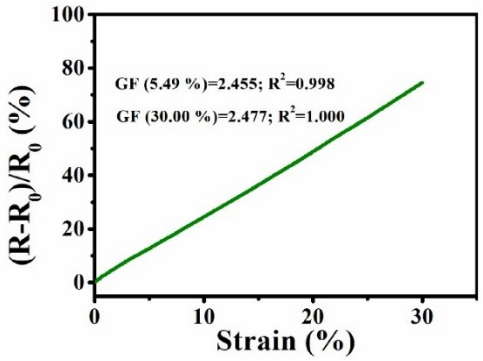

Fig. S14 Relative resistance changes and GF with the increase of tensile strain of self-healed GDIH10-0.06.

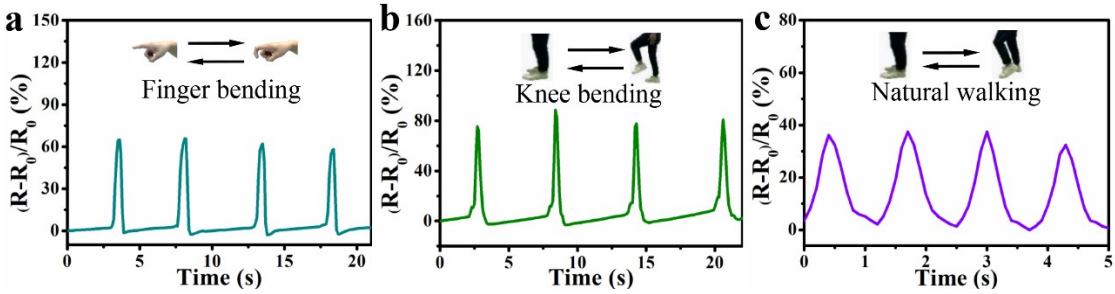

Fig. S15 The recorded relative resistance changes of the sensor made of the self-healed hydrogel (GDIH10-0.06) for (a) forefinger bending and (b, c) knee bending, respectively.

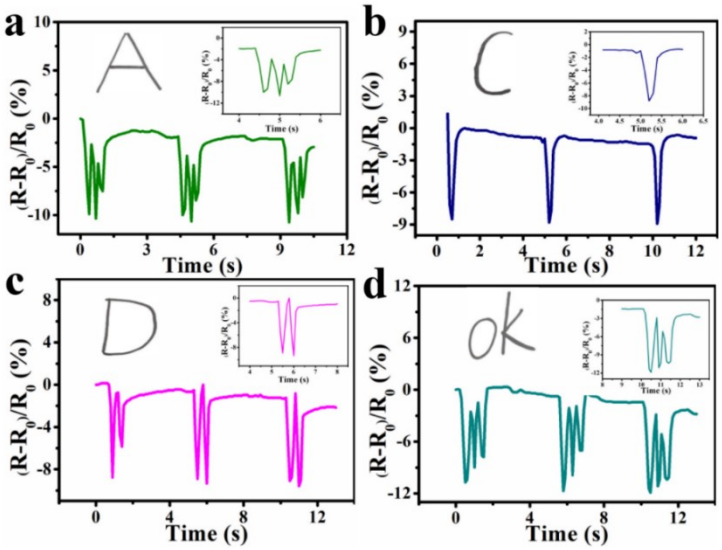

Fig. S16 Relative resistance changes of the self-healed GDIH10-0.06 on writing "A", "C", "D", "ok".

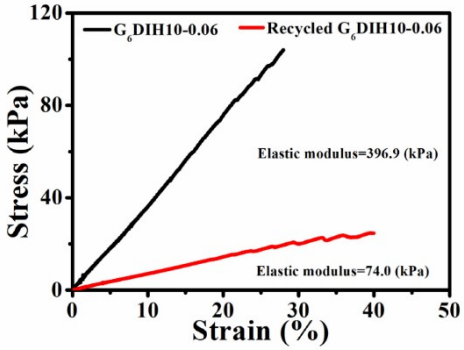

Fig. S17 The tensile strength of G_6DIH10-0.06 and recycled G_6DIH10-0.06.

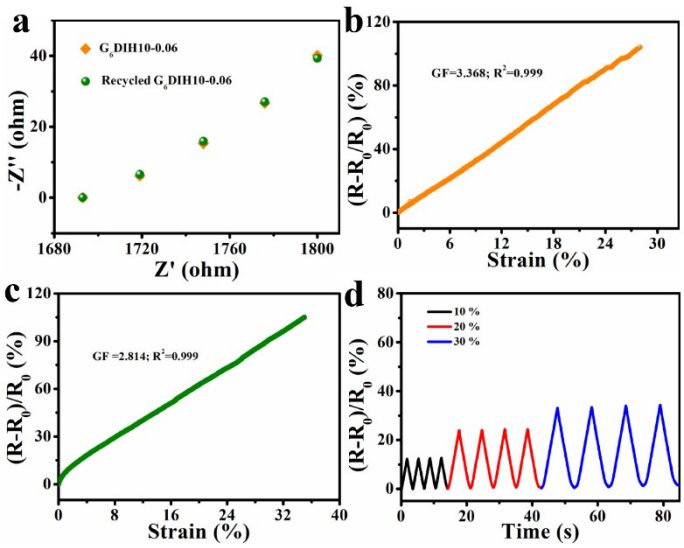

Fig. S18 (a) EIS plots of G_6DIH10-0.06 and recycled G_6DIH10-0.06. The GF of (b) G_6DIH10-0.06 and (c) recycled G_6DIH10-0.06. (d) Time-dependent relative resistance changes with different tensile strains of recycled G_6DIH10-0.06.

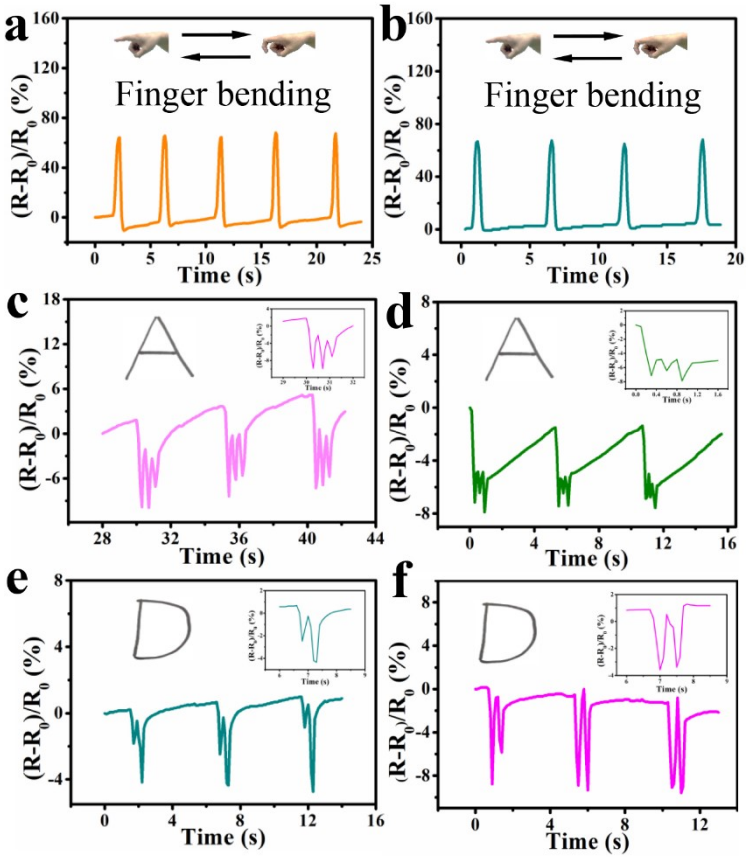

Fig. S19 The sensing performance of G_6DIH10-0.06 (left) and recycled G_6DIH10-0.06-based sensor (right): (a, b) Relative resistance changes of sensor for forefinger bending. (c-f) Relative resistance changes of sensors on writing “A” and “D”.

Fig. S20 Photos of abandoned GDIH10-0.06 in water at different times under 45 °C. The abandoned GDIH10-0.06 can easily dissolve in water after 20 min.

The adhesion strength of our adhesive, glue stick and glue on surfaces of copper and paper was presented in Fig. S21. The adhesion performance of our adhesive was higher than that of glue when two copper was staggered, which was similar to that of glue stick when the paper was adhered.

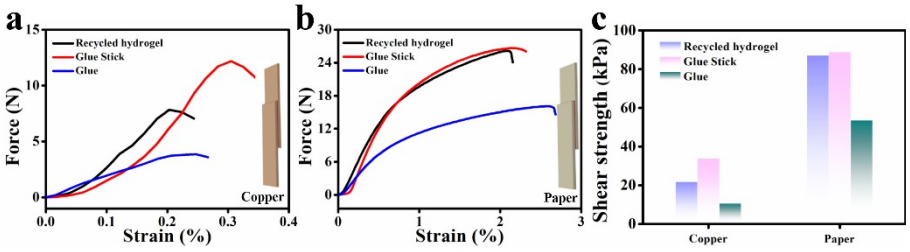

Fig. S21 Comparison of adhesion strength between our adhesive, glue stick and glue on surfaces of copper and paper.

Table S1 The carboxyl content, aldehyde content and crystallinity index (CrI) of TNFC and DATNFC.

Sample	Carboxyl content mmol/g	Aldehyde content mmol/g	CrI %
TNFC	0.33	/	69.7
DATNFC	/	2.55	66.9

Table S2 The T_{50} (temperature at 50% mass loss), T_{max} (maximum degradation rate temperature) and residual mass of nanocomposite hydrogel.

Sample	T_{50}/ °C	T_{max}/ °C	Residual mass/%
GDH10	356.2	342.3	24.6
GDIH10-0.02	362.9	320.5	30.6
GDIH10-0.04	375.1	316	33.1
GDIH10-0.06	378.4	314.8	33.8
GDIH10-0.08	382.7	315.9	34.8
GDIH10-0.10	384.0	318.5	35.3

Video S1.mp4

Video S1 The brightness of LED lamp with different pressure.

Video S2.mp4

Video S2 The adhesion property of GDH10.

Video S3.mp4

Video S3 The adhesion property of GDIH10-0.06.

References

1. J. Yang, F. Xu and C. R. Han, *Biomacromolecules.*, 2017, **18**, 1019-1028.
2. L. Bi, Z. Cao, Y. Y. Hu, Y. Song, L. Yu, B. Yang, J. H. Mu, Z. S. Huang and Y. S. Han, *J. Mater. Sci.: Mater. Med*., 2011, **22**, 51–62.
3. C. Sheng, Y. M. Zhou, X. Y. Zhang and G. X. Xue, *Fibers Polym.*, 2018, **9**, 2030-2038.
4. C. Liu, Y. Hou, Y. M. Li, and H. N. Xiao, *J. Colloid Interface Sci.*, 2022, **614**, 566-573.
5. Q. M. Yan, M. Zhou and H. Q. Fu, 2020, *J. Mater. Chem. C.*, 8, 7772-7785.
6. J. Kang, J. B. H. Tok and Z. N. Bao, 2019, *Nat. Electron.*, **2**, 144-150.
7. J. P. Li, L. Kang, B. Wang, K. F. Chen, X. J. Tian, Z. Ge, J. S. Zeng, J. Xu and W. H. Gao, *ACS Sustainable Chem. Eng.*, 2018, **7**, 1146-1158.
8. B. Sun, Q. X. Hou, Z. H. Liu and Y. H. Ni, *Cellulose.*, 2015, **22**, 1135-1146.
9. Q. X. Liu, J. Liu, S. F. Qin, Y. Pei, X. J. Zheng and K. Y. Tang, *Int. J. Biol. Macromol.*, 2020, **164**, 1776-1784.
10. R. Dash, M. Foston and A. J. Ragauskas, *Carbohydr. Polym.*, 2013, **91**, 638-645.
11. L. Kang, L. J. Shi, Q. Zeng, B. K. Liao, B. Wang and X. P. Guo, *Sep. Purif. Technol.*, 2021, 279, 119737.
12. P. F. Li, J. S. Zeng, B. Wang, Z. Cheng, J. Xu, W. H. Gao and K. F. Chen, *Carbohydr. Polym.*, 2020, **247**, 116721.
13. H. X. Zhu, W. Guo, J. Wang, H. He, X. D. Hou, S. J. Zhou and S. F. Wang, *Cellulose.*, 2019, **26**, 9149-9161.
14. J. N. Wu, L. Chen, T. Fu, H. B. Zhao, D. M. Guo, X. L. Wang and Y. Z. Wang, *Chem. Eng. J.*, 2018, **336**, 622-632.
15. H. Q. Zhang, Z. J. Liu, J. P. Mai, N. Wang, H. J. Liu, J. Zhong and X. M. Mai, *Adv. Sci.*, 2021, **8**, 2100320.
16. R. A. Li, G. X. Chen, M. H. He, J. F. Tian and B. Su, *J. Mater. Chem. C.*, 2017, **5**, 8475-8481.
17. C. Dang, M. Wang, J. Yu, Y. Chen, S. H. Zhou, X. Feng, D. T. Liu and H. S. Qi,

Adv. Funct. Mater., 2019, **29**, 1902467.

18. C. Dang, F. Peng, H. C. Liu, X. Feng, Y. Liu, S. N. Hu and H. S. Qi, *J. Mater. Chem. A.*, 2021, **9**, 13115-13124.